

Journal of Materials Chemistry A

Accepted Manuscript



This is an *Accepted Manuscript*, which has been through the Royal Society of Chemistry peer review process and has been accepted for publication.

Accepted Manuscripts are published online shortly after acceptance, before technical editing, formatting and proof reading. Using this free service, authors can make their results available to the community, in citable form, before we publish the edited article. We will replace this *Accepted Manuscript* with the edited and formatted *Advance Article* as soon as it is available.

You can find more information about *Accepted Manuscripts* in the [Information for Authors](#).

Please note that technical editing may introduce minor changes to the text and/or graphics, which may alter content. The journal's standard [Terms & Conditions](#) and the [Ethical guidelines](#) still apply. In no event shall the Royal Society of Chemistry be held responsible for any errors or omissions in this *Accepted Manuscript* or any consequences arising from the use of any information it contains.

Enhanced Adsorption of Dibenzothiophene with Zinc/Copper-Based Metal-Organic Frameworks

Tingting Wang,^a Xingxian Li,^a Wei Dai,^{*a} Yaoyao Fang,^a and He Huang^b

^aCollege of Chemistry and Life Science, Zhejiang Normal University, Zhejiang Province Jinhua 321004, People's Republic of China

^bCollege of Biotechnology and Pharmaceutical Engineering, Nanjing University of Technology, Nanjing 210009, People's Republic of China

[#]Xingxian Li equally contributed to this work as Tingting Wang, and they are both the first author.

ABSTRACT: A novel type of bimetallic-organic porous material (Zn/Cu-BTC) has been successfully synthesized with Zn²⁺ replacing Cu²⁺ in the paddle wheel unit. The as-synthesized sorbents were characterized with XRD, SEM, ICP, and TGA analyses and N₂ adsorption at 77 K. The desulfurization performance of the prepared adsorbents was evaluated by the selective adsorption of dibenzothiophene (DBT) from the simulated oils in a fixed-bed breakthrough column at room temperature (298K). From the obtained breakthrough curves, both the breakthrough capacity and the saturation capacity of the adsorbents for sulfur element were determined. The results shown that Zn/Cu-BTC exhibited high desulfurization capacities, which are even superior to those reported previously in the literatures. In addition, these novel adsorbents possessed good durability and affinities for the adsorption of dibenzothiophene in the presence of aromatic components and moisture. The saturated adsorbent Zn/Cu-BTC can be regenerated with nitrogen atmosphere sweeping at 573 K for 5 h. More than 90 % of the desulfurization capacity was recovered after regeneration.

Key words: Metal-organic frameworks; Adsorption; Dibenzothiophene; Zn/Cu-BTC

1. Introduction

Desulfurization of liquid hydrocarbon fuels has attracted increasing attention due to adverse environmental impacts of sulfur oxides present in engine exhaust emissions.¹ According to United States and European Union regulations, the acceptable sulfur contents in commercial fuels are limited to 15 and 10 $\mu\text{g/g}$, respectively.^{2,3} The traditional industrial process is hydro-desulfurization (HDS), which is effective for aliphatic and acyclic S-compounds but less effective for thiophenic compounds (a typical sulfur compound is the dibenzothiophene).⁴ To achieve ultra-deep desulfurization, some non-HDS alternative technologies such as adsorption desulfurization,^{5,6} extractive desulfurization,^{7,8} bio-desulfurization,⁹ oxidative desulfurization,^{10,11} and others^{12,13} have been proposed. Among the non-HDS alternative technologies, adsorptive purification might be one of the most competitive methods to reduce sulfur content up to ultralow values due to some advantages, such as mild operation conditions and no need for hydrogen or oxygen.¹⁴

Very recently, MOF-type materials have also been investigated for the adsorptive removal of hazardous materials such as benzene, dyes, and sulfur compounds.¹⁵⁻²⁰ A few important factors, such as coordinatively unsaturated sites,²¹ pore functionalities,¹⁹ and acid-based interactions¹⁷ have been suggested for the efficient adsorptive removal of sulfur compounds with MOFs. However, the most widely studied crystalline MOFs are usually constructed from a small number of distinct building blocks, and thus relatively “simple” in terms of their composition and

structure.

Mixed-component metal-organic frameworks (MC-MOFs) have different linkers or metals with the same structural role. Many of these mixed-ligand or mixed-metal MOFs are solid solutions, in which the proportions of the ligands or metals can be adjusted or even controlled. These MC-MOFs can be prepared directly, using more than one metal or ligand in the synthesis, or formed by post-synthetic modification.²² A second class of MC-MOFs have core-shell structures, which can be prepared through epitaxial growth of one MOF on the surface of another or post-synthetic modification of the crystal surfaces. Recently, some of these MC-MOFs have been reported, namely block crystals and core-shell MOF structures, developed by Kitagawa and their co-workers.²³ Solid-solution MOFs, which can be regarded as molecularly substitutional alloys, and multivariate metal-organic porous materials, introduced by Yaghi and co-workers,¹⁹ are other attractive types of mixed-component MOFs. These materials can be prepared directly by using more than one metal or ligand in the hydrothermal method or formed by post-synthetic modification. The possibilities of introducing advanced complexity into MOF materials hold enormous potential due to the ability to adjust or even control the ratios of the organic and inorganic components in the structure, providing novel control over pore metrics and compositions and, hence, tailoring in a particular way the physicochemical properties beyond the options available to the single-component parent MOFs. For example, increasing the capacity of selective adsorption and improving the selective adsorption of adsorbate and the catalytic activity have been achieved.²³ The major applications

currently being considered for these MC-MOFs mostly focus on gas storage, catalysis, separations, as carriers for nano-materials and drug delivery. Recently, adsorptive removal of sulfur-containing compounds by MOFs has received attention because of the maturity of methods for MOFs preparation. Khan et al.²⁴ used three similar MOFs, MIL-47(V) and MIL-53(Al, Cr), as adsorbents to remove benzothiophene. In their investigation of the kinetics and thermodynamics of benzothiophene adsorption, they found that the role of the metal center in MOFs in adsorption is significant and that the process is an acid–base interaction. Cunha et al.²⁵ investigated the influence of the metal ions in MIL-100 (Al^{3+} , Cr^{3+} , Fe^{3+} , and V^{3+}) on the adsorptive removal of N/S heterocyclic molecules from fuels. Among the various MOFs, Cu–BTC also known as HKUST-1 is one of the well-known MOFs with high surface area and pore volume, having outstanding properties in gas storage, separation, catalysis, and magnetism.¹⁶ Petit et al.²⁶ found that reactive adsorption occurred and resulted in the formation of copper sulfide when Cu-BTC was used for adsorption of hydrogen sulfide. However, the study about the adsorption desulfurization by MC-MOFs is still relative scarce.²⁷

It is well known that Zn and Cu are adjacent position in periodic table of elements, and they have the similar features such as atomic quantity (Cu: 63.55, Zn: 65.39), atomic radius (Cu: 135(145) pm, Zn: 135(142) pm), electron configuration (Cu: $[\text{Ar}]3d^{10}4s^1$, Zn: $[\text{Ar}]3d^{10}4s^2$).²⁸ The paddle wheel complex built from the axial Cu^{2+} and Zn^{2+} ions and 1,3,5-benzenetricarboxylic acid (H_3BTC), is very interesting because of its easy preparation, flexibility and open metal site. The choice of Zn and Cu is based on the expected higher affinity for thiophene molecule, according to their

adsorption behavior in Zn/Cu MC-MOFs. An alternative strategy for forming a zinc/copper MC-MOM is to substitute some of the copper metal centers by zinc metal in a post-synthetic modification reaction. This is schematically shown in Scheme S.I.1.

In this work, we report the adsorptive removal of DBT as a typical organosulfur compound with our MOFs consisting of two different central metals (Cu^{2+} and Zn^{2+}) and the same organic ligand (H_3BTC). To the best of our knowledge, this is the first study to utilize double metals as π -complexation active sites for the purpose of adsorptive removal of organosulfur compounds. Commercial oil products contain different portions of aromatic components, therefore, three simulated oils with different amounts of aromatic components were prepared in this study i.e. 100 wt % aromatic component (ARO), 20 wt % aromatic component (MIO) and 100 wt % aliphatic component (ALO). The desulfurization behavior of the novel Zn/Cu-BTC desulfurizer was investigated and compared in a fixed-bed breakthrough column at room temperature (298K) and atmospheric pressure.

2. Experimental

2.1 Adsorbent Preparation

The synthesis of Cu-BTC was synthesized using a slightly modified solvothermal method and synthesis procedure as described in detail elsewhere.^{16,29} Briefly, an exact amount of H_3BTC (Sigma Aldrich, 98%, 2.0 mmol) and copper (II) nitrate trihydrate ($\text{Cu}(\text{NO}_3)_2 \cdot 3\text{H}_2\text{O}$, Wako pure chemicals industry Ltd., 99%, 3.65 mmol) was dissolved in 24 mL of a 1:1 (wt./wt.) mixture of water and ethanol, and stirred

magnetically for 10 min. The resulting reactant mixtures were loaded into a Teflon autoclave, sealed and placed in a microwave oven (Mars-5, CEM, maximum power of 1200 W) to take advantage of rapid synthesis under microwaves.³⁰⁻³² After the reaction for 1.0 h at 413 K, the autoclaves were allowed to cool down to room temperature and then the solid products were recovered with centrifugation. The solid products were washed with a water-ethanol mixture to remove any unreacted H₃BTC and dried overnight at 373 K. Zn/Cu-BTC materials were synthesized by following the same procedure but using Zn(NO₃)₂·6H₂O as a zinc source in order to substitute 35, 55 and 75 % molar Cu by Zn source.

2.2 Characterization techniques

The powder X-ray diffraction pattern (XRD) of the synthesized samples were recorded on a Bruker D8 Advance X-ray Diffractometer with Cu K α radiation under 40 kV and 200 mA in the scan range of 2θ from 5° to 90° with a scan step of 0.02°. Scanning electron microscopy images were obtained from a scanning electron microscope (Philips PW 3040/60) operated at 20 kV. Prior to the observation, the sample was sputter-coated with a gold layer to increase their conductivity. The textural properties of the synthesized MOFs were determined from the nitrogen adsorption-desorption isotherms recorded at 77 K with an automated adsorption apparatus (Micromeritics, ASAP2020). Prior to the measurement of nitrogen isotherms, all samples were previously degassed under vacuum at 423 K for about 24 h. The specific areas of the samples were determined according to standard BET procedure using nitrogen adsorption data taken in the relative equilibrium pressure

(P/P_0) range between 0.05 and 0.2 and with a value of 0.162 nm^2 for the cross-section of adsorbed nitrogen molecule. The total pore volume was estimated to be the liquid N_2 volume at a relative pressure of 0.99. The pore size distributions were determined using the density functional theory (DFT) method for slit-shaped pores. Metal contents of the synthesized materials were measured by ICP (Inductively Coupled Plasma) atomic emission spectroscopy on a Varian Vista AX CD system. The samples were previously dissolved in concentrated sulfuric acid and subsequently calcined at 573 K to eliminate the organic part, being the resulting residual solid dissolved in a sulphuric acid solution and analyzed by ICP. Thermogravimetric analysis was performed using a Netzsch STA 449 C instrument and experiments were conducted with a constant heating rate of 278 K /min in nitrogen atmosphere.

2.3 Desulfurization of sorbents

Three simulated oils were prepared using benzene (99.8 %, Sigma-Aldrich) as the representative of aromatic oil (ARO), n-octane (99.8 %, Sigma-Aldrich) as the representative of aliphatic oil (ALO), and the mixture of 80 wt % n-octane and 20 wt % benzene was used to represent the mixed oil (MIO). DBT (>99 %, Sigma-Aldrich) was used as the representative of sulfur contaminants. The content of sulfur element in the simulated oils for ARO, ALO and MIO are $760 \mu\text{g/g}$, $760 \mu\text{g/g}$ and $190 \mu\text{g/g}$, respectively. The desulfurization performance of adsorbents was tested on the basis of breakthrough curves. Experiments to collect the breakthrough curves were performed in a vertical quartz column of length 100 mm and inner diameter of 5 mm with a glass grid for supporting the adsorbent. The sorbents were loaded into the

adsorption column inside a glove box to avoid contact with air. The testing oil was pumped up with a mini creep pump (BT01-YZ1515). Prior to each adsorption measurement, the adsorbent was activated by being heating to 423 K and maintained for 2 h in nitrogen stream. After cooling to room temperature (298 K) in a nitrogen stream, the sorbent was consolidated by light tapping. The adsorption experiments were carried out at 298 K and atmospheric pressure. First, the fixed bed was flushed downward with sulfur-free n-octane or benzene at a flowrate of 1 cm³/min for 30 min, and then the feed was switched to the simulated oils containing different contents of DBT with unchanged flowrate. Samples were taken regularly to examine the sulfur content in the simulated oils until saturation was reached. The total sulfur content in the simulated oils was determined with a gas chromatograph GC-7890 (Shanghai Science Instrument Co., Ltd.) equipped with a flame photometric detector and an EC-5 capillary column (length = 40 m; i.d. = 0.32 m). Sulfur concentrations were determined from the calibrated sulfur standard curves. Breakthrough curves were obtained by plotting the transient sulfur concentration versus the cumulative fuel volume. The concentration was normalized with the total sulfur content in the feed, and the cumulative fuel volume was normalized with the volume of the adsorbent bed. The normalized sulfur adsorption capacity of an adsorbent was calculated with the following equations (1) and (2):

$$q_b = \left(\frac{v\rho x_i}{m}\right) \times t_b \times 100\% \quad (1)$$

$$q_s = \left(\frac{v\rho x_i}{m}\right) \int_0^{t_s} \left[1 - \frac{c_t}{c_i}\right] dt \times 100\% \quad (2)$$

Where q_b is the breakthrough capacity per unit mass of adsorbent, %; q_s is the

saturation capacity of unit mass of adsorbent, %; v is the flowrate of oil, cm^3/min ; ρ is the fuel density, g/cm^3 ; c_i is the initial sulfur content, ppm; c_t is the sulfur content of the oil passing through the bed at time t , ppm; m is the mass of adsorbent in the column, g; x_i is the content of sulfur element in the simulated oils, %; t_b is the breakthrough time, min; t_s is the saturation time when $c_t/c_i=1$, min.

3. Results and discussion

3.1 Properties of the adsorbents

The nitrogen adsorption isotherms and the pore size distribution curves of Cu-BTC, Zn35/Cu-BTC, Zn55/Cu-BTC, and Zn75/Cu-BTC at 77 K are shown in Fig. 1 and Fig. 2. The BET surface area and pore volume were obtained from nitrogen physisorption isotherms at 77 K, and the results are given in Table S.I.1. As shown in Fig.1 and Table S.I.1, the nitrogen adsorption isotherms of all the MOFs including the virgin Cu-BTC are similar to one another and have type I isotherms, indicating the microporosities of the adsorbents. The total pore volumes of Cu-BTC, Zn35/Cu-BTC, Zn55/Cu-BTC, and Zn75/Cu-BTC are 0.62, 0.59, 0.57 and 0.52 cm^3/g , respectively. The pore size distributions calculated by density functional theory (DFT) prove that the pore size of Cu-BTC and Zn/Cu-BTC ranges from 1 to 2 nm. It is clear that incorporation of Zn^{2+} into the Cu-BTC decreased the MOFs surface area. The BET surface area of the four MOFs samples follows the order Cu-BTC>Zn35/Cu-BTC>Zn55/Cu-BTC>Zn75/Cu-BTC. Zn/Cu-BTC are constructed by the self-assembly of organic ligands (H_3BTC) and metal-containing nodes Zn^{2+} and Cu^{2+} . To explain the reduced surface area with increasing zinc content, one has to realize that the square

planar coordination environment of the metal cation present in $\text{Cu}_3(\text{BTC})_2$ is not the favorable one for zinc. This may result in an increased defect concentration of the isolated material; i.e., structural domains do not show the perfect crystallographic $\text{Cu}_3(\text{BTC})_2$ structure and therefore prevent the full formation of the 3D porosity and lead to a reduced surface area. Such finding is similar to that made in previous works on MC-MOFs.^{33,34}

To identify the structure of the material, the crystallinity of Cu-BTC and Zn/Cu-BTC were probed by Powder X-ray diffraction (Fig. 3). Zn/Cu-BTC appears isostructural to Cu-BTC, with a slightly larger unit cell. The patterns were indexed using on the basis of a face-centered cubic unit cell with the resultant values of $a=b=c=26.353\pm 0.001$ and $a=b=c=26.532\pm 0.001\text{\AA}$ for Cu-BTC and Zn55/Cu-BTC, respectively. Differences in peak intensities could be attributed to pore occlusion by molecular guests. The results are similar to previously reported in the literature.^{33,34,35} The results qualitatively support Zn incorporation into the framework (Ionic radius size of Zn^{2+} and Cu^{2+} are similar) and are in good agreement with theoretical calculations for a Zn-doped Cu-BTC framework. Cu-BTC and Zn/Cu-BTC are very similar and also very close to the corresponding values derived for the as-synthesized. Because of the almost identical electron density, X-ray diffraction cannot readily distinguish between Zn^{2+} and Cu^{2+} within the dinuclear units in the frameworks. Therefore, in the crystal structure determination, the metal atoms were randomly distributed at the same sites in the lattice with a relative Zn/Cu ratio (occupation factor). In order to observe its surface morphology, the images of Cu-BTC and

Zn55/Cu-BTC were taken with a scanning electron microscope (SEM) after gold deposition. As illustrated in Fig. 4, two samples show very similar features, suggesting that Zn-doping does not change the morphology of crystal structure. The crystals sample of Zn55/Cu-BTC in SEM image had a double-sided pyramidal shape with about 10~20 μm in width. Such regular structure confirmed the good crystallization which was already testified by its powder X-ray diffraction pattern. The chemical composition of evacuated Zn-containing materials was determined by ICP spectroscopy and elemental analysis, resulting the following materials: a) $\text{Zn}_{0.9}\text{Cu}_{2.1}(\text{BTC})_2$ (sample named Zn35/Cu-BTC); b) $\text{Zn}_{1.5}\text{Cu}_{1.5}(\text{BTC})_2$ (sample named Zn55/Cu-BTC); and c) $\text{Zn}_{2.4}\text{Cu}_{0.6}(\text{BTC})_2$ (sample named Zn75/Cu-BTC).

On the basis of TGA results (Fig. 5), the first step of weight loss in the temperature range 30~120 $^{\circ}\text{C}$ can be attributed to the loss of moisture and solvent molecules. The second step is due to the decomposition of organic linkers. From 373 to 573 K, no obvious mass loss can be found, which demonstrated the prepared MOFs should be heated under a stream of nitrogen below 573 K, the temperature at which the structure severely collapsed. Further increasing the temperature to 623 K, the weight of Cu-BTC and Zn55/Cu-BTC decreased about 50 and 60 %, respectively. Slight mass loss can be found when temperature was further increased to 623 K. Compared to that of pure Cu-BTC, the second weight loss of Zn55/Cu-BTC occurs in lower temperature. The behavior also indicates that zinc ions might locate in the framework; otherwise, it would be difficult to rationalize such a pronounced effect of the presence of zinc ions on the decomposition temperature of the organic linkers. Specifically,

trials were performed at activation temperatures of 393 K. After treatment, the samples were cooled in nitrogen to ambient temperature to further remove DBT.

3.2 Desulfurization capacities of as-prepared MOFs

DBT breakthrough curves of Cu-BTC and Zn/Cu-BTC samples were recorded and shown in Fig. 6, 7 and 8 for ALO, ARO and MIO, respectively. For all three simulated oils, Zn/Cu-BTC sorbents adsorbed more DBT than Cu-BTC due to more stronger π -complexation reaction (Synergistic ability of double metals (Zn^{2+} and Cu^{2+}) are stronger than single metal (Cu^{2+}), but the uptake amounts are not proportional to the doping amount of Zn^{2+} . This non-linear response could be a consequence of variations in the structure and composition of domains on the Zn/Cu-BTC surface, or inaccessibility to the active Zn^{2+} and Cu^{2+} sites for some domains. Shapes of the curves can provide qualitative information about the strength of adsorption. For example, the steeper slopes for the Zn/Cu-BTC sorbents suggested their stronger interactions with DBT than Cu-BTC does. It was found that the sulfur uptake capacity of Zn/Cu-BTC was significantly increased in comparison with the Cu-BTC, which is due to more stronger π -complexation between DBT and active sites. Further increasing the Zn^{2+} doping level increases the amount of the active Zn^{2+} sites, which results in the better desulfurization capacity of Zn55/Cu-BTC than Zn35/Cu-BTC. While if more Zn^{2+} were introduced into the support, it may block the pore and leads to the increase of the diffusion resistance during the mass transfer reactions, which actually can decrease the amount of accessible active sites to form the π -complexation with DBT, and thus the sorbent with higher Zn^{2+} loading (Zn75/Cu-BTC) shows a

smaller sulfur uptake capacity than that with lower Zn^{2+} loading (Zn35/Cu-BTC and Zn55/Cu-BTC). Therefore, among all the samples, Zn55/Cu-BTC shows the highest desulfurization capacity. Another thing that should be noted is that Zn/Cu-BTC sorbents have better desulfurization performance for ALO than for ARO. For example, the maximal breakthrough capacity and saturation capacity of the Zn55/Cu-BTC are 9.93 and 11.89 wt % for ALO, while the corresponding values reduce to 4.98 and 5.92 wt % for ARO with respect to the sulfur element. Although the capacity decreased, the adsorbent still shows better desulfurization performance than those previously reported.^{36,37} The breakthrough capacities of the adsorbents in this work are summarized in Table 2, together with some other π -complexation sorbents reported previously.^{4,36,37} Breakthrough capacities for some of the Zn/Cu-BTC sorbents were comparable or superior to those of activated carbons, zeolites, SBA-15 and MOF-5/Cu(I) reported previously.^{4,36,37}

On the other side, the Zn/Cu-BTC adsorbents show much stronger durability in desulfurization with the presence of the dissolved water. In order to test the effect of moisture in the oil on the desulfurization capacity of the sorbents, water-saturated simulated oil was prepared as follows: Simulated MIO oil containing 80 wt % n-octane, 20 wt % benzene, and DBT (190 ppm sulfur element) was mixed and thoroughly agitated with distilled water and the mixture sat until distinct oil and water phases appear, the water-saturated simulated oil can be obtained after getting rid of the water phase. The DBT breakthrough curves were then collected using dry and water-saturated simulated oil (MIO), and the results are shown in Fig. 9. The

breakthrough and saturation capacity of the Zn55/Cu-BTC adsorbent for the sulfur element are 7.21 and 7.93 wt % in the dry oil, but the corresponding values reduced to 6.67 and 7.08 wt % in the water-saturated oil. Although the capacity decreased 7.49 % and 10.72 % respectively for breakthrough and saturation capacity with the presence of water in the oil, these performances are still much better than the sorbents reported previously.^{4,37,38} To avoid the loss of desulfurization capacity caused by water, a layer of high surface area carbons made from Finger Citron Residue-Based Activated Carbons³⁴ (FACs) was put on the top of Zn55/Cu-BTC, then DBT breakthrough curve were tested using the water-saturated oil. By this way, the dissolved water in the oil could be adsorbed by the layer of activated carbon before the oil contacts with the Zn55/Cu-BTC. Excluding the amount of DBT adsorbed by activated carbon, the breakthrough and saturation adsorption capacity of Zn55/Cu-BTC were calculated to be 7.16 and 7.88 wt %, respectively, which is quite close to the adsorption capacities of the adsorbent in the dry oil. Therefore, the effect of dissolved water on the adsorption capacity of the Zn/Cu-BTC adsorbent can be easily eliminated by adding extra layer of FACs.

3.3 Regeneration performance of as-prepared Zn/Cu-BTC

The adsorbents are required to be regenerative for multiple cycles to reduce the adsorbent cost. Generally, the adsorbed DBT could not be removed from the Zn/Cu-BTC materials by purging with sulfur-free n-octane. However, DBT can elute from Zn/Cu-BTC during a similar purge. Preliminary experiments also indicated that regeneration of the Zn/Cu-BTC sorbents required high temperature treatment. These

results are consistent with strong interactions between DBT and adsorption sites on the π -complexation. The π -complexation adsorption mechanism has been proposed for the adsorption of organosulfur compounds.³¹⁻³⁴ The color of Zn/Cu-BTC is black when it is saturated with DBT. After the nitrogen sweeping at 573 K for 5 h, Zn55/Cu-BTC recovered its original light blue color. The DBT breakthrough curves of regenerated Zn55/Cu-BTC were then collected again with the three types of simulated oil, and the results shown that the sulfur uptake capacities of the regenerated adsorbent in these oils are all higher than 90 % of the initial values. Taking MIO for example (Fig. 10), the sulfur uptake capacities of the regenerated Zn55/Cu-BTC are 6.49 % for breakthrough capacity, and 7.37 % for saturation capacity, which are more than 90% and 93% of the initial values, respectively. In view of practical application, the XRD patterns, nitrogen adsorption isotherms were measured and compared in Fig. S.I.1, S.I.2 and S.I.3, respectively. The results shown that the XRD patterns of Zn/Cu-BTC before and after adsorption/desorption experiment were well matched and their surface area and pore volume were similar each other, which indicates that the stability of Zn/Cu-BTC is satisfactory during the desulfurization process. Similar results were also investigated in the literatures.^{4,27} As a whole, the as-prepared adsorbents, i.e., Zn55/Cu-BTC, can be easily regenerated after the adsorption desulfurization process and recycled five times at least.

4. Conclusions

Partial doping of the Cu-BTC with a metal Zn^{2+} has been successfully carried out. Characteration of this bimetallic-organic porous material was confirmed by XRD,

TGA, SEM, ICP and N₂ adsorption. The Zn/Cu-BTC materials prepared have higher adsorption capacities for DBT from ALO, ARO and MIO model oils. The adsorption results support the assumption that zinc is actually incorporated into the framework and that it plays an important role in the desulfurization process, even being incorporated into unexposed metal sites that are less accessible to DBT molecules. Stronger durability in the presence of aromatic components and moisture was also observed, and the effect of dissolved water on the adsorption capacity of the adsorbent can be easily eliminated using a layered column of activated carbon at the top of Zn/Cu-BTC sorbents. Besides the high desulfurization capacity, Zn/Cu-BTC sorbents can be easily regenerated by nitrogen sweeping and about 90 % of the sulfur uptake capacity was recovered after regeneration. This study opens the possibility of doping different MOFs with a variety of metal ions during solvothermal crystallization, with the aim of improving their adsorption properties for environmental and energy applications, as well as for other potential applications in the fields of adsorption separation.

Corresponding Author

*^aE-mail: daiwei@zjun.edu.cn. Fax: +86-579-82282531. Tel:+86-579-82282269.

Acknowledgements

This work was supported by the Public Projects of Zhejiang Province of China (No. 2015C31083), Zhejiang Qianjiang Talent Project (No. QJD1302014) and The Financial Support by Open Research Fund of Top Key Discipline of Chemistry in Zhejiang Provincial Colleges and Key Laboratory of the Ministry of Education for

Advanced Catalysis Materials (Zhejiang Normal University).

Notes and references

- 1 Y. Shi, X. Zhang, L. Wang and G. Liu, *AIChE J.*, 2014, **60**, 2747–2751.
- 2 A. Samokhvalov and B. J. Tatarchuk, *Catal. Rev. Sci. Eng.*, 2010, **52**, 381–410.
- 3 A. Stanislaus, A. Marafi and M. S. Rana, *Catal. Today*, 2010, **153**, 1–68.
- 4 W. Dai, J. Hu, Li. Zhou, S. Li, X. Hu and He. Huang, *Energy Fuels*, 2013, **27**, 816-821.
- 5 P. Jeevanandam, K. J. Klabunde and S. H. Tetzle, *Microporous Mesoporous Mater.*, 2005, **79**, 101–110.
- 6 X. Gao, H. Mao, M. Lu, J. Yang and B. Li, *Microporous Mesoporous Mater.*, 2012, **148**, 25–33.
- 7 Y. Nie, C. Li and Z. Wang, *Ind. Eng. Chem. Res.*, 2007, **46**, 5108–5122.
- 8 A. Revelli, F. Mutelet, J. Jaubert, *J. Phys. Chem. B.*, 2010, **114**, 4600–4608.
- 9 Z. A. Irani, M. R. Mehrnia, F. Yazdian and M. Soheily, *Bioresour. Technol.*, 2011, **102**, 10585–10591.
- 10 D. P. Morales, A. S. Taylor and S. C. Farmer, *Molecules*, 2010, **15**, 1265–1269.
- 11 S. Kumar, V. C. Srivastava and R. P. Badoni, *Fuel Process. Technol.*, 2012, **93**, 18–25.
- 12 B. R. Fox, B. L. Brinich, J. L. Male, R. L. Hubbard, M. N. Siddiqui, T. A. Saleh and D. R. Tyler, *Fuel*, 2015, **156**, 142–147.
- 13 B. Guo, R. Wang and Y. Li, *Fuel*, 2011, **90**, 713–718.
- 14 W. Dai, R. Gong, J. Hu and L. Zhou, *Sep. Sci. Tech.*, 2014, **49**, 367–375.

- 15 S. H. Jung, J. H. Lee, J.W. Yoon, C. Serre, G. Férey and J. S. Chang, *Adv. Mater.*, 2007, **19**, 121–124.
- 16 J. Hu, H. Yu, W. Dai, X. Yan, X. Hu and H. Huang, *RSC Adv.*, 2014, **4**, 35124–35130.
- 17 N. A. Khan, J. W. Jun, J. H. Jeong and S. H. Jung, *Chem. Commun.*, 2011, **47**, 1306–1308.
- 18 N.A. Khan and S. H. Jung, *Angew. Chem. Int. Ed.*, 2012, **51**, 1198–1201.
- 19 A. R. Millward, O. M. Yaghi, *J. Am. Chem. Soc.*, 2005, **127**, 17998–17999.
- 20 U. Mueller, M. Schubert, F. Teich, H. Puetter, K. Schierle-Arndt and J. Pastré, *J. Mater. Chem.*, 2006, **16**, 626–636.
- 21 S. Achmann, G. Hagen, M. Hämmerle, I. Malkowsky, C. Kiener, R. Moos, *Chem. Eng. Technol.*, 2010, **33**, 275–280.
- 22 H. Hou, G. Li, L. Li, Y. Zhu, X. Meng and Y. Fan, *Inorg. Chem.*, 2003, **42**, 428–435.
- 23 K. Hirai, S. Furukawa, M. Kondo, H. Uehara, O. Sakata and S. Kitagawa, *Angew. Chem. Int. Ed.*, 2011, **50**, 8057–8061.
- 24 Z. Hasan and S. H. Jung, *J. Hazard. Mater.*, 2015, **283**, 329–339.
- 25 D. Cunha, J. S. Lee, J. S. Chang, E. Gibson, M. Daturi, J. C. Lavalley, A. Vimont, I. Beurroies, D. E. De Vos, *J. Am. Chem. Soc.*, 2013, **135**, 9849–9856.
- 26 C. Petit, B. Levasseur, B. Mendoza and T. J. Bandoz, *Microporous Mesoporous Mater.*, 2012, **154**, 107–112.
- 27 Y. Li, L. Wang, H. Fan,, S. Ju, H. Wang, and J. Mi, *Energy Fuels*, 2015, **29**,

- 298–304
- 28 C. Guminski, *Pure Appl. Chem.*, 2015, **87**, 477–485.
- 29 S. S. Y. Chui, S. M. F. Lo, J. P. H. Charmant, A. G. Orpen and I. D. Williams, *Science*, 1999, 283, 1148–1150.
- 30 N. A. Khan, E. Haque and S. H. Jung, *Phys. Chem. Chem. Phys.*, 2010, **12**, 2625–2631.
- 31 N. A. Khan and S. H. Jung, *Cryst. Growth Des.*, 2010, **10**, 1860–1865.
- 32 E. Haque, N. A. Khan, J. H. Park and S. H. Jung, *Chem. A Eur. J.*, 2010, **16**, 1046–1052.
- 33 J.I. Feldblyum, M. Liu, D. W. Gidley and A. J. Matzger, *J. Am. Chem. Soc.*, 2011, **133**, 18257–18263.
- 34 F. Gul-E-Noor, B. Jee, M. Mendt, D. Himsl, A. Pöpl, M. Hartmann, J. Haase, H. Krautscheid and M. Bertmer, *J. Phys. Chem. C*, 2012, **116**, 20866–20873.
- 35 J. Hafizovic, M. Bjørgen, U. Olsbye, P. D. C. Dietzel, S. Bordiga, C. Prestipino, C. Lamberti and K. P. Lillerud, *J. Am. Chem. Soc.*, 2007, **129**, 3612–3620.
- 36 R. T. Yang, A. J. Hernandez-Maldonado and F. H. Yang, *Science*, 2003, **301**, 79–81.
- 37 W. Dai, Y. Zhou, S. Li, W. Li, W. Su, Y. Sun and Li. Zhou, *Ind. Eng. Chem. Res.*, 2006, **45**, 7892–7896.
- 38 R. T. Yang and A. J. Hernandez-Maldonado, *Ind. Eng. Chem. Res.*, 2003, **42**, 123–129.

Figure captions:

Fig. 1 N₂ adsorption–desorption isotherms of Cu-BTC and Zn/Cu-BTC samples at 77 K.

Fig. 2 Pore size distribution of Cu-BTC and Zn/Cu-BTC samples.

Fig. 3 XRD analysis for Cu-BTC and Zn55/Cu-BTC samples

Fig. 4 SEM images of Zn55/Cu-BTC samples.

Fig. 5 TGA of Cu-BTC and Zn55/Cu-BTC samples under nitrogen atmosphere.

Fig. 6 Breakthrough curves of dibenzothiophene in the aliphatic oil over Cu-BTC and Zn/Cu-BTC at room temperature.

Fig. 7 Breakthrough curves of dibenzothiophene in the aromatic oil over Cu-BTC and Zn/Cu-BTC at room temperature.

Fig. 8 Breakthrough curves of dibenzothiophene in the mixed oil over Cu-BTC and Zn/Cu-BTC at room temperature.

Fig. 9 Breakthrough curves of DBT in the MIO feed over the Zn55/Cu-BTC adsorbent at room temperature. a: water-saturated; b: without water; c: Zn55/Cu-BTC packed together with FACs.

Fig. 10 Breakthrough curves of DBT over the regenerated composite adsorbent Zn55/Cu-BTC in MIO. a: Breakthrough capacity, wt %; b: Saturation capacity, wt %.

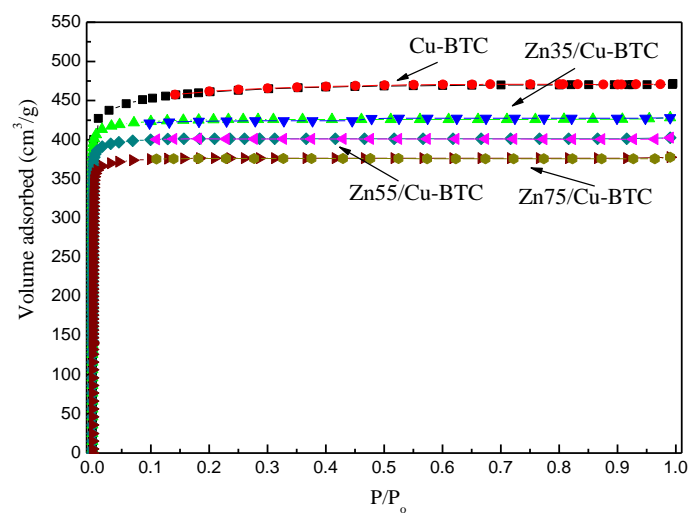


Fig. 1 N₂ adsorption–desorption isotherms of Cu-BTC and Zn/Cu-BTC samples at 77 K.

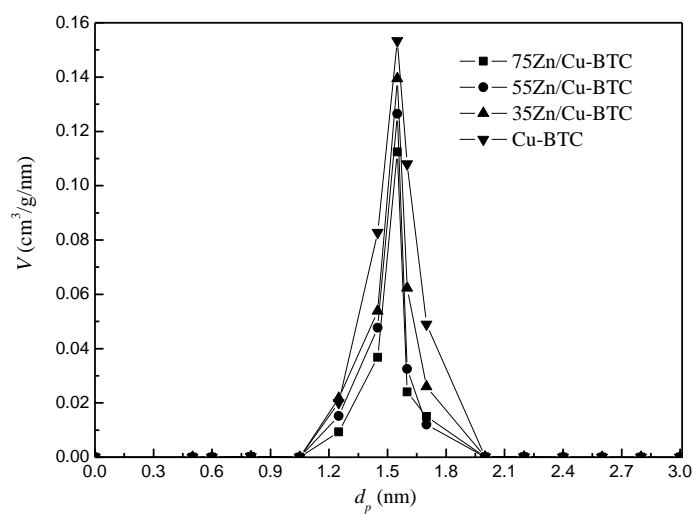


Fig. 2 Pore size distributions of Cu-BTC and Zn/Cu-BTC samples.

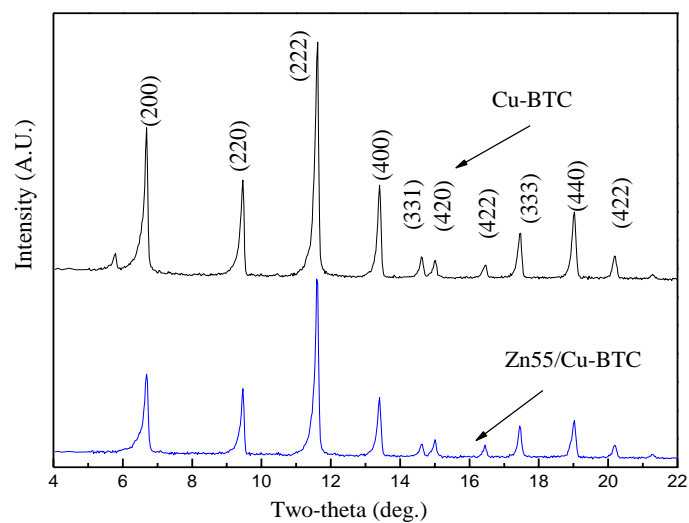


Fig. 3 XRD analysis for Cu-BTC and Zn55/Cu-BTC samples

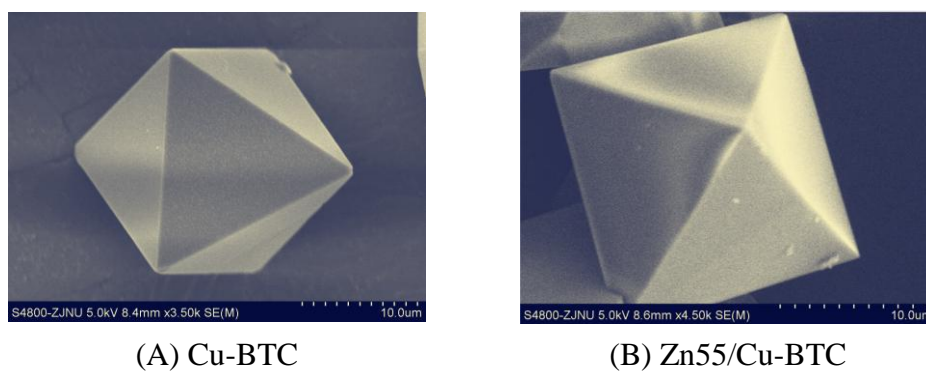


Fig. 4 SEM images of Cu-BTC and Zn55/Cu-BTC samples, respectively.

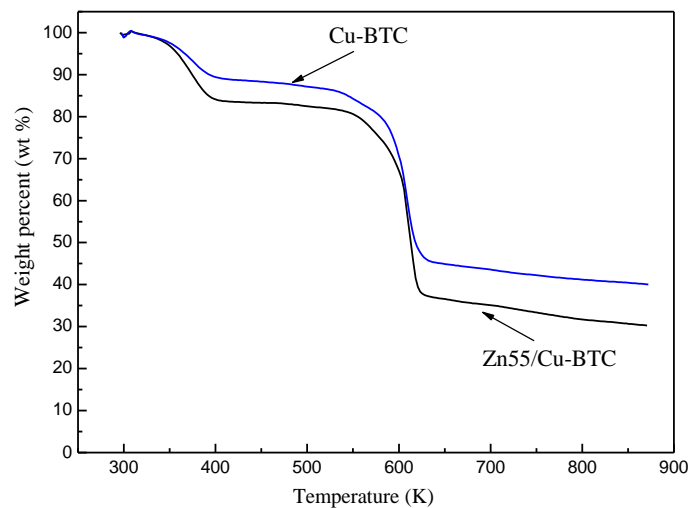


Fig. 5 TGA of Cu-BTC and Zn55/Cu-BTC samples under nitrogen atmosphere.

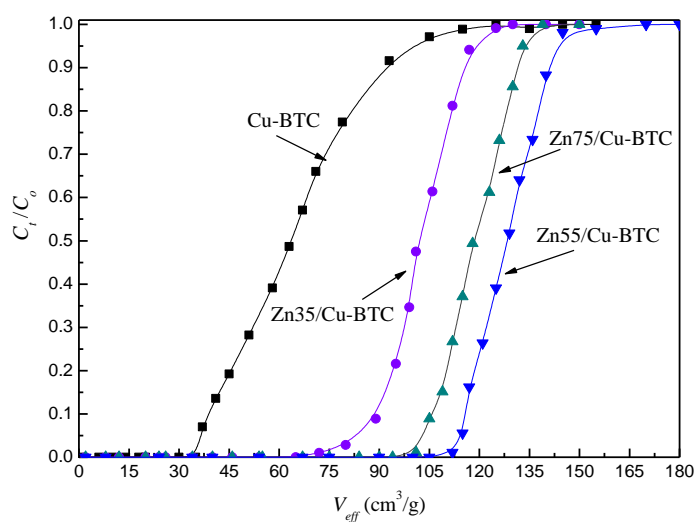


Fig. 6 Breakthrough curves of dibenzothiophene in the AIO over Cu-BTC and Zn/Cu-BTC at room temperature.

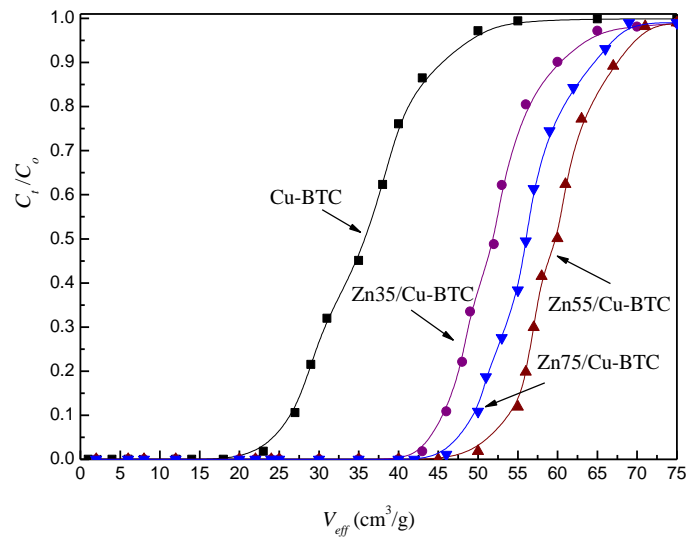


Fig. 7 Breakthrough curves of dibenzothiophene in the ARO over Cu-BTC and Zn/Cu-BTC at room temperature.

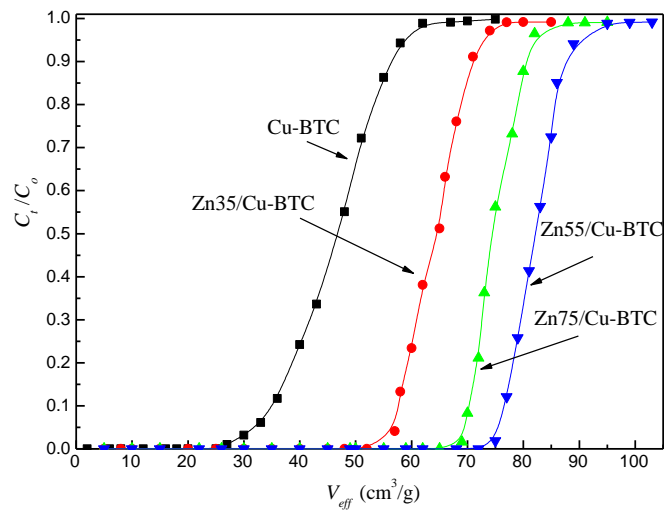


Fig. 8 Breakthrough curves of dibenzothiophene in the MIO over Cu-BTC and Zn/Cu-BTC at room temperature.

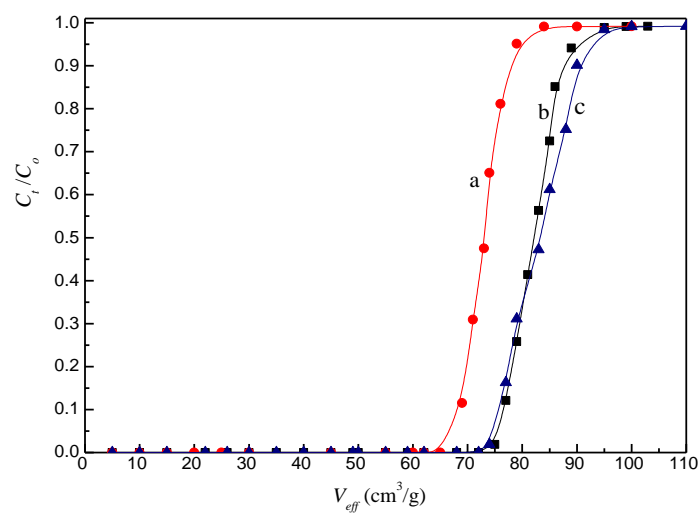


Fig. 9 Breakthrough curves of DBT in the MIO feed over the Zn55/Cu-BTC adsorbent at room temperature. a: water-saturated; b: without water; c: Zn55/Cu-BTC packed together with FACs.

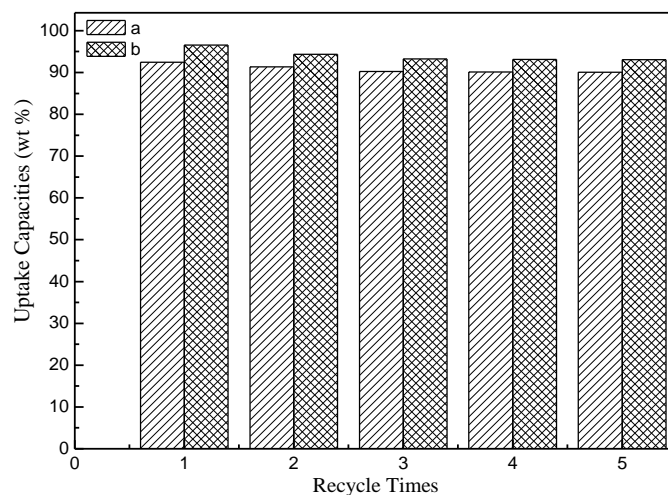


Fig. 10 Breakthrough curves of DBT over the regenerated adsorbent Zn55/Cu-BTC in MIO. a: Breakthrough capacity, wt %; b: Saturation capacity, wt %.

A table of contents entry:

Enhanced Adsorption of Dibenzothiophene with Zinc/Copper-Based Metal-Organic Frameworks

Tingting Wang,^a Xingxian Li,^a Wei Dai,^{*a} Yaoyao Fang,^a and He Huang^b

^aCollege of Chemistry and Life Science, Zhejiang Normal University, Zhejiang Province Jinhua 321004, People's Republic of China

^bCollege of Biotechnology and Pharmaceutical Engineering, Nanjing University of Technology, Nanjing 210009, People's Republic of China

[#]Xingxian Li contributed with Tingting Wang, and they are both the first author.

A novel type of bimetallic-organic porous material (Zn/Cu-BTC) plays an important role in the adsorption desulfurization.

